

Analytical Model Methodology Development and Demonstration of Approach on Used Fuel Performance Characterization for Condition of Normal Transportation – 14568

Kenneth Geelhood *, Harold Adkins *, Scott Sanborn *, Brian Koeppel *, Nicholas Klymyshyn*
* Pacific Northwest National Laboratory

ABSTRACT

U.S. Nuclear Regulatory Commission (NRC) rules require that used nuclear fuel (UNF) rods maintain their integrity during handling, transportation, and storage to ensure maintenance of the fuel retaining boundary, safety against criticality, and long term fuel retrievability for processing and disposal. Consequently, understanding the mechanical performance of UNF rods under cumulative loading stemming from handling, normal conditions of transport (NCT), and normal conditions of storage (NCS) is necessary as their performance under these conditions establishes part of their safety basis.

The U.S. Department of Energy (DOE) commissioned a multi-laboratory team consisting of subject matter experts at Pacific Northwest National Laboratory, Idaho National Laboratory, Sandia National Laboratories, and Oak Ridge National Laboratory to develop a methodology to examine the structural performance and potential for failure of UNF under NCT and to perform a demonstration of this methodology for a typical UNF transportation campaign. This team prepared a Research, Development, and Demonstration (RD&D) Plan that describes a methodology, including development and use of analytical models, to evaluate loading and associated mechanical responses of UNF rods and key structural components during NCT. The initial scope of this plan has now been fully executed. The demonstration of the methodology laid out in the RD&D plan is focused on structural performance evaluation of Westinghouse Electric 17x17 OFA pressurized water reactor fuel assemblies with a discharge burnup range of 30-58 GWd/MTU (assembly average), loaded in a representative high-capacity (≥ 32 fuel rod assemblies) transportation package and transported on a 3000 mile rail journey.

In general, the modeling and simulation approach consists of three levels; the cask level, the fuel assembly level, and the fuel rod level. This modeling approach utilized finite element analysis sub-modeling techniques to accurately model the complete spent nuclear fuel transport system on the railcar (cask restraint structure, cask, basket, assembly, and fuel rods). The sub-modeling approach allows for more detailed finite element models of individual system components, faster analysis run times for the individual sub-models, and flexibility when updating or modifying the sub-models to incorporate better excitation data, initial material properties, or other pertinent information.

The final results of the initial demonstration are that cladding strains were not large enough to cause structural failure, but cyclic strains roughly projected for the entire route were significant in some cases. The number of cycles that the model hits certain strain "bins" are counted. These are extrapolated for a 3000 mile trip and the damage ratio is calculated which is the number of cycles the fuel rods hit certain strain bins over the 3000 mile journey divided by the number of cycles to failure. Under the final model and set of inputs, the total damage from summation of the worst shock and vibration cases is ~18% of the expected fatigue limit. Therefore the fuel rods are not expected to fail during NCT given the assumptions listed. Additionally, a number of sensitivity studies were performed. It was found that the areas of highest sensitivity were the cladding elastic modulus, the spacer grid stiffness, the spacer grid location, and gaps between the

assembly and the cask; these findings can be used to guide future work.

INTRODUCTION

The U.S. Department of Energy (DOE) commissioned a multi-laboratory team consisting of subject matter experts at Pacific Northwest National Laboratory (PNNL), Idaho National Laboratory (INL), Sandia National Laboratories (SNL), and Oak Ridge National Laboratory (ORNL) as well as private sector firms (TTCI) to develop a methodology to examine the structural performance and potential for failure of UNF under NCT and to perform a demonstration of this methodology for a typical UNF transportation campaign. This team prepared a RD&D Plan that describes a methodology, including development and use of analytical models, to evaluate loading and associated mechanical responses of UNF rods and key structural components during NCT. This plan has now been fully executed. The demonstration of the methodology laid out in the RD&D Plan, is focused on structural performance evaluation of Westinghouse Electric 17x17 OFA pressurized water reactor fuel assemblies with a discharge burnup range of 30-58 GWd/MTU (assembly average), loaded in a representative high-capacity (≥ 32 fuel rod assemblies) transportation package and transported on a 3000 mile rail journey.

This paper will describe the modeling approach that was selected, identification of the modeling inputs, the model validation, and results of the initial demonstration. Additionally, sensitivity analyses on various input parameters and modeling assumptions were performed to identify those areas with significant impact on the final results. These sensitivity analyses will be used to guide future work to refine models and inputs in areas that are most important. The results of this effort are fully described elsewhere [1].

MODELING APPROACH

The general modeling approach is shown schematically in Fig. 1 along with the identified data inputs and outputs. In general, the modeling and simulation approach consists of three levels; the cask level [2], the fuel assembly level [3], and the fuel rod level [4]. This modeling approach utilized finite element analysis sub-modeling techniques to accurately model the complete spent nuclear fuel transport system on the railcar (cask restraint structure, cask, basket, and fuel assemblies). The sub-modeling approach allows for more detailed finite element models of individual system components, faster analysis run times for the individual sub-models, and flexibility when updating or modifying the sub-models to incorporate better excitation data, initial material properties, or other pertinent information.

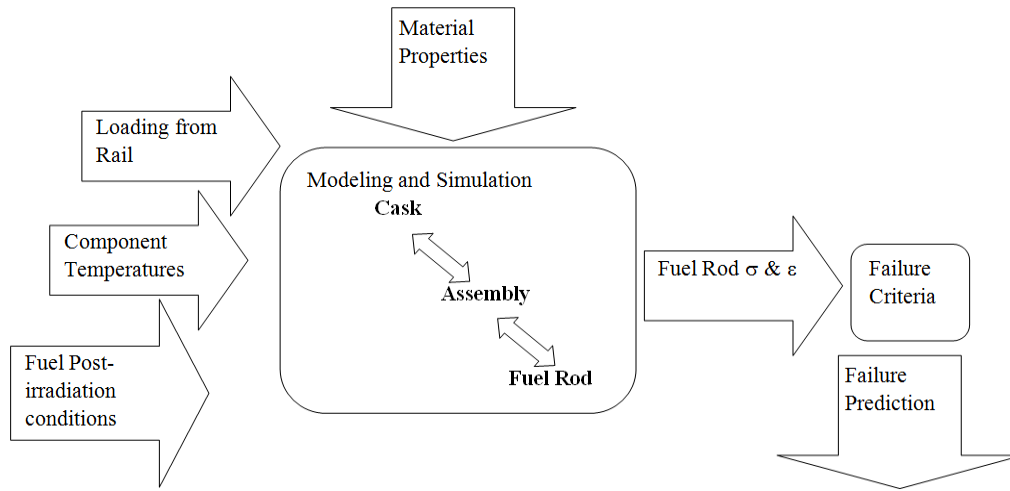


Fig. 1. Overview of Modeling Approach with Inputs and Outputs

There are four major inputs to the models identified in Fig. 1. The loading from the rail-transport feeds into the cask modeling effort by using excitations from the railcar bed. Typical shock and vibration accelerations were provided to the team from Transportation Technology Center Inc. (TTCI) using their NUCARS[®] program. The provided accelerations were validated against calculations performed for existing acceleration data taken on a similar rail car. A consistent set of material properties were documented and used at all modeling levels. Best estimate models taken from vetted NRC fuel performance codes were used for the irradiated fuel and cladding properties. Typical component temperatures were calculated and used consistently in the modeling. Finally, fuel post-irradiation conditions were established for various burnup levels and used in the modeling.

All levels of sub-modeling used input component temperatures, fuel post-irradiation conditions and material properties from a common source as appropriate. The excitation loads from the rail interface are used to define the boundary conditions for the fully loaded cask model. The system dynamics are then sequentially evaluated at the cask level, fuel assembly level, and fuel rod level. Finally, the predicted loads and deformations on the fuel rods are output for failure evaluation. Two failure criteria were initially established. One was for fatigue loading for loads that caused very little or no plastic deformation. The second was for loads that caused significant plastic deformation. The results of the models indicated that the maximum loads were significantly less than the yield stress which made the second criterion unnecessary. To validate the fatigue failure criterion, data on irradiated and unirradiated samples from the literature were collected, and new fatigue test data on unirradiated samples with surrogate bonded and un-bonded pellets was produced at ORNL [5]. These data demonstrate that selected fatigue failure criterion represents the current best fatigue failure limit for UNF under NCT. Fig. 2 shows the irradiated data and the fatigue failure curve. Work is ongoing at ORNL to produce data from bend tests on actual irradiated fuel rod segments. These data will be used to provide further validation for the current fatigue failure limit.

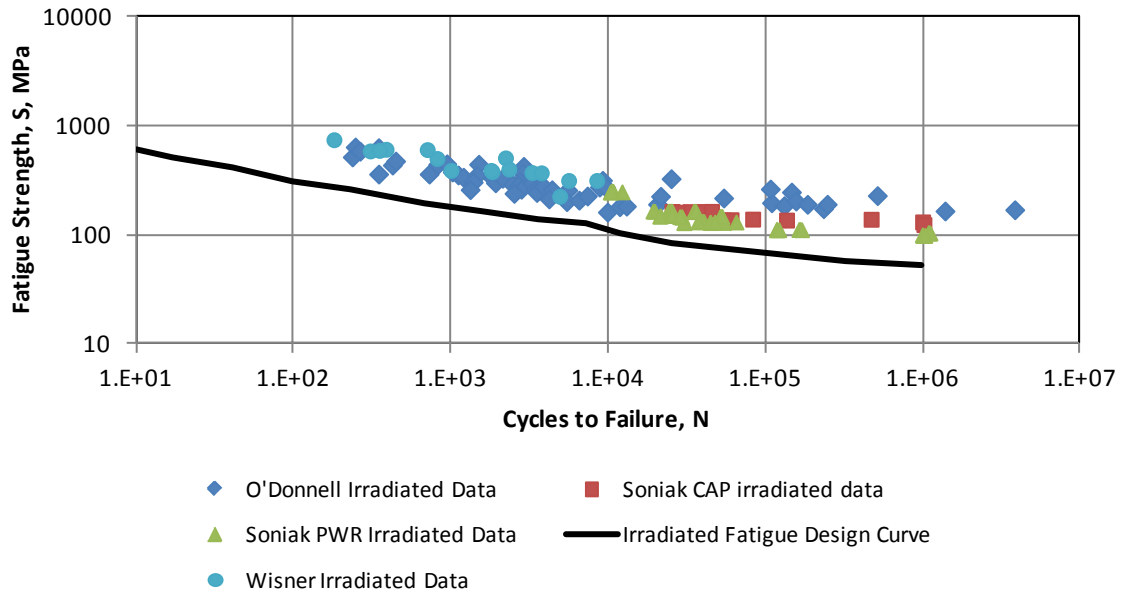


Fig. 2. All Irradiated Fatigue Data and Irradiated Fatigue-Design Curve Applicable To Used Nuclear Fuel under NCT

MODELING INPUTS

Fig. 1 shows four main modeling inputs. A fifth modeling input is the geometry of the fuel assemblies, cask, and rail car. This section will discuss the selection of each of these input parameters for the initial demonstration.

Geometry

As previously mentioned the initial demonstration was performed using Westinghouse Electric 17×17 OFA pressurized water reactor fuel assemblies with a discharge burnup range of 30-58 GWd/MTU (assembly average), loaded in a generic burnup cask (GBC) -32 transportation package described in NUREG/CR-6747 [6].

The geometry for the rail car conveyance, cask, canister, basket, fuel assemblies, and fuel rods were defined and a consistent set of values was used for the modeling at three distinct levels. Fig. 3 shows model overviews of these components at different levels.

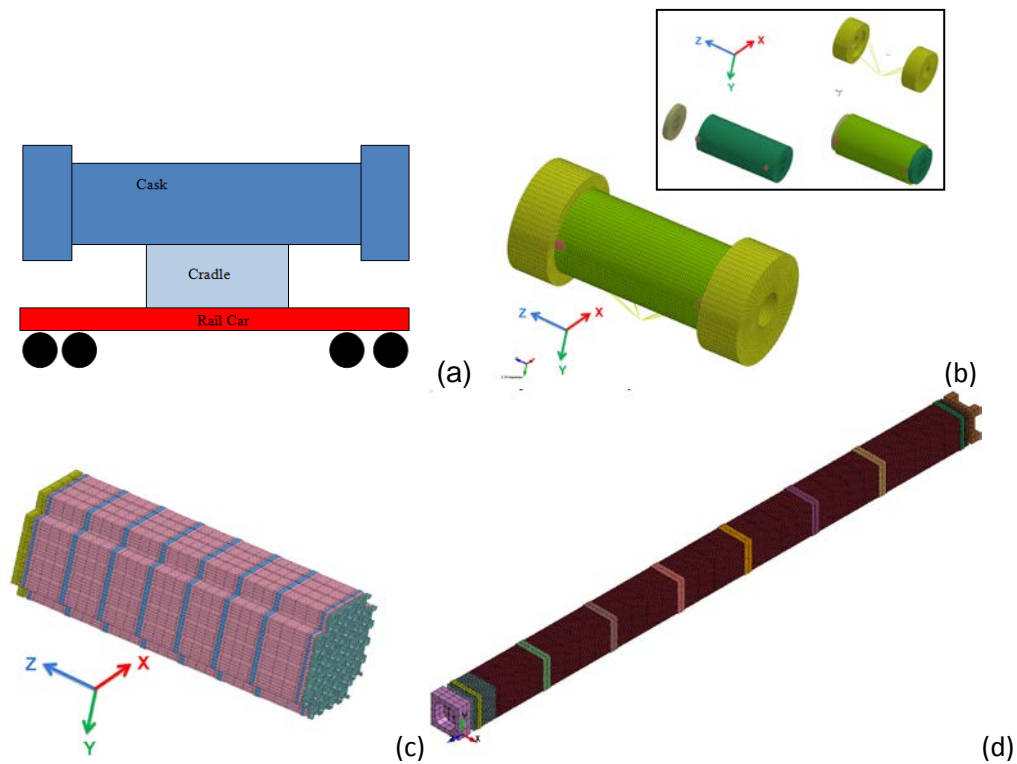


Fig. 3. Model Overview of (a) Rail Car Conveyance, (b) Cask and Cask Components, (c) Basket and Fuel Assemblies, and (d) Single Fuel Assembly

Material Properties

Material property correlations for irradiated fuel, cladding, and other assembly components (e.g., grid spacers) have been provided in the Material Properties Handbook [7] that was developed under this initiative. This document also includes material property correlations for the materials in the generic burnup cask (GBC)-32.

The most critical material properties are the properties of zirconium-based cladding and UO_2 fuel in the irradiated conditions. The correlations presented in the Material Properties Handbook were taken from the NRC fuel performance codes FRAPCON-3 [8] and FRAPTRAN [9] which are well vetted and supported by an extensive database. Correlations for zirconium based cladding as a function of temperature and level of irradiation were provided for elastic modulus, yield stress, ultimate tensile strength, uniform plastic elongation, fracture toughness, fatigue, and density. Correlations for sintered UO_2 fuel pellets as a function of temperature and burnup were provided for elastic modulus, fracture strength, and density. The grid straps in the OFA can be made from Zircaloy or Inconel, and correlations were provided for both of these materials for elastic modulus, yield stress, ultimate tensile strength, total elongation and density.

Material properties were also provided for the cask materials including 304 stainless steel, 316 stainless steel, XM-19 steel, Boral, and Al-1100. The casks will not be irradiated. Correlations for these materials as a function of temperature were provided for elastic modulus, yield stress, ultimate tensile strength, total elongation, and density.

Component Temperatures

A preexisting ANSYS model was utilized to calculate approximate temperatures of various components in a Holtec HI-STAR 100 with an MPC-24 containing Westinghouse Electric 17x17 OFA fuel assemblies [10]. These temperatures are sufficiently representative of the GBC-32 because of the moderate thermal influence on thermal material properties of the packaging and payload components. These temperature calculations were performed as a function of decay heat within the fuel assembly payload and ambient temperature outside the package. Component temperatures are provided for two limiting cases. The maximum heat load with a high ambient temperature will provide upper bound component temperatures. The minimum heat load with a low ambient temperature will provide lower bound component temperatures.

The maximum decay heat load case used a total distributive heat load of 20 kW and an ambient temperature of 38°C which represents the upper limit that can be transported by the system on a normal hot day per 10 CFR 71.71. The minimum heat load case used a heat load of 2.7 kW and an ambient temperature of -29°C which represents fuel cooled for 300 years and transported on a normal cold day per 10 CFR 71.71. Average and maximum component temperatures for each of these cases were tabulated and used consistently at the various model levels.

Fuel Post-Irradiation Conditions

In addition to providing MP correlations for the components in the fuel assemblies and the GBC-32, the Material Properties Handbook [7] also contains a section that provides representative conditions of fuel rods as a function of burnup and axial location. These conditions include burnup level, fast neutron fluence, corrosion layer thickness and hydrogen content. All of these parameters are input values to various correlations described in the Material Properties Handbook [7]. These tables were used as necessary to provide initial conditions for the fuel rods being modeled under this initiative.

TABLE I shows typical conditions at 1-ft intervals for the peak fuel rod from assemblies discharged at 55 GWd/MTU assembly average burnup. These tables were developed with calculations from FRAPCON-3.4 [8]. No fuel cladding gap is predicted in moderate-to-high burnup fuel when cooled to room temperature. The contact pressure is removed, but there is no effective gap predicted beyond the sum of the fuel and cladding roughness (about 2.5 μm). The conditions shown in these tables are for the peak rod in the assembly. These conditions were conservatively used for all of the rods in an assembly.

TABLE I. Typical Conditions for Peak Fuel Rod from PWR Westinghouse Electric 17x17 OFA Fuel Assembly Discharged at Assembly Average Burnup of 55 GWd/MTU

PWR Westinghouse 17x17 Fuel Assembly											
		Assembly Average Burnup		55 GWd/MTU		Cladding material: Zircaloy-4					
		Peak Rod Average Burnup		58.87 GWd/MTU		Peak Rod Fast Neutron Fluence		9.85E+25 n/m ²			
Upper Plenum		Gas Composition 84.0% He, 13.6% Xe, 2.4% Kr				Total void volume = 10.94 cm ³			Total Gas = 2.0E-2 Moles		
		<u>Local</u>	<u>Local Fast</u>	<u>Corrosion</u>	<u>Metal</u>	<u>Hydrogen</u>	<u>Excess</u>	<u>Excess</u>	<u>Excess</u>	<u>Excess</u>	<u>Excess</u>
		<u>Burnup</u>	<u>Neutron</u>	<u>layer</u>	<u>Consumed</u>	<u>Concentration</u>	<u>Hydrogen</u>	<u>Hydrogen</u>	<u>Hydrogen</u>	<u>Hydrogen</u>	<u>Hydrogen</u>
		<u>GWd/MTU</u>	<u>n/m²</u>	<u>Thickness</u>	<u>um</u>	<u>ppm</u>	<u>@ 20°C</u>	<u>@ 100°C</u>	<u>@ 200°C</u>	<u>@ 300°C</u>	<u>@ 400°C</u>
node 12		45.1 ^l	7.55E+25 ^l	62.8 ^l	40.3 ^l	522 ^l	522 ^l	521 ^l	509 ^l	457 ^l	322 ^l
node 11		57.1 ^l	9.56E+25 ^l	79.7 ^l	51.1 ^l	666 ^l	666 ^l	665 ^l	653 ^l	601 ^l	466 ^l
node 10		62.7 ^l	1.05E+26 ^l	82.1 ^l	52.6 ^l	687 ^l	687 ^l	686 ^l	674 ^l	622 ^l	487 ^l
node 9		63.8 ^l	1.07E+26 ^l	67.2 ^l	43.1 ^l	560 ^l	560 ^l	559 ^l	547 ^l	495 ^l	360 ^l
node 8		63.8 ^l	1.07E+26 ^l	57 ^l	36.5 ^l	474 ^l	474 ^l	473 ^l	461 ^l	409 ^l	274 ^l
node 7		63.7 ^l	1.07E+26 ^l	45.9 ^l	29.4 ^l	381 ^l	381 ^l	380 ^l	368 ^l	316 ^l	181 ^l
node 6		63.6 ^l	1.07E+26 ^l	39.2 ^l	25.1 ^l	326 ^l	326 ^l	325 ^l	313 ^l	261 ^l	126 ^l
node 5		63.5 ^l	1.06E+26 ^l	32.1 ^l	20.6 ^l	267 ^l	267 ^l	266 ^l	254 ^l	202 ^l	67 ^l
node 4		63.4 ^l	1.06E+26 ^l	26.4 ^l	16.9 ^l	221 ^l	221 ^l	220 ^l	208 ^l	156 ^l	21 ^l
node 3		62 ^l	1.04E+26 ^l	20.2 ^l	12.9 ^l	171 ^l	171 ^l	170 ^l	158 ^l	106 ^l	0 ^l
node 2		54.7 ^l	9.16E+25 ^l	14.2 ^l	9.1 ^l	123 ^l	123 ^l	122 ^l	110 ^l	58 ^l	0 ^l
node 1		43.1 ^l	7.21E+25 ^l	8.4 ^l	5.4 ^l	77 ^l	77 ^l	76 ^l	64 ^l	12 ^l	0 ^l

It is acknowledged that the conditions described here are those of the fuel rod immediately upon discharge from the reactor. It is possible that the conditions of vacuum drying (up to 400°C) and extended dry cask storage (20°C to 400°C for 20 to 60 years) could change the MP and initial conditions provided in the Material Properties Handbook.

One possibility includes hydride reorientation due to the vacuum drying operations which was not accounted for. Typically the hydrides in PWR Zircaloy-4 cladding are circumferentially oriented and primarily located in a dense hydride rim along the outer edge of the cladding. If a significant number reorient to the radial direction, it can cause brittle failure to occur in the cladding by providing an easy path for a crack to propagate through the cladding thickness. When hydride reorientation is observed, brittle failure has been observed before yielding of the clad occurs. Work is currently underway on this initiative and other initiatives to evaluate if hydride reorientation has occurred in fuel currently being stored in dry casks, and if so, what the impact on failure or ductility is. The possibility of hydride reorientation will not be examined in the modeling work under the current initiative, although the results of the modeling work for this initiative can be used to assist in assessing the impact of hydride reorientation if it is found to have occurred.

Another possibility includes low temperature/long-term annealing of the irradiation damage in the cladding. Irradiation damage significantly increases the strength of Zircaloy-4 and slightly increases the elastic modulus of Zircaloy-4. If this damage is annealed out, the strength and modulus could be reduced and approach their unirradiated values. Sensitivity studies were performed to address the impact of low temperature/long-term annealing following extended dry

cask storage.

One of the sensitivities that was performed is to evaluate the impact of clad thinning due to in-reactor fretting on the potential for failure. In order to perform this sensitivity, it should be assumed that the cladding could be up to 10% thinner in the locations contacted by the springs and dimples on the grid spacers.

One other initial condition is the degree of fuel-clad bonding that has occurred during in-reactor service. It is known that at moderate to high burnup, a fuel-clad bonding layer forms. However, the properties of this layer such as strength or effective friction coefficient are poorly characterized. Therefore, one of the sensitivity studies assessed the impact of this uncertainty by evaluating the case with no fuel-clad bonding, and the case with perfect fuel-clad bonding.

Loading from Rail

In the RD&D Plan [11] an approach for obtaining shock and vibration data was developed. This data was used to determine the effects of the shock and vibration associated with the rail-related NCT on UNF assemblies and rods. The option chosen used the extensive data archives and simulation capabilities of TTCL in a three-step process:

1. Obtain existing data for a representative railcar.
2. Use the NUCARS[®] program [12] to simulate a representative railcar.
3. Use the NUCARS[®] program to simulate a representative UNF railcar carrying a generic current generation rail transportation cask.

The data provided from task 2 was processed as the Phase 1 Loads and was used in the initial modeling work. The data from task 3 was processed as the Phase 3 Loads and was used in the final modeling work.

Phase 1 (P1) loads were extracted from a set of data files received from TTCL on July 8, 2013. Each data file contained an approximately six-minute-duration snapshot of measured acceleration time-history data for two separate rail cars in a single train, taken from a much larger data set of measurements spanning several days and hundreds of miles of track traveled. TTCL performed the initial culling of the larger data set to provide six-minute-duration data snapshots in which large accelerations were observed in the measured accelerations in each of the three directions (axial – along the length of the track, lateral, and vertical). Nineteen unique snapshots were provided for each car, meaning a total of thirty-eight unique snapshots were provided. Data for each car consisted of three-axis acceleration measurements obtained at each end of the rail car. The accelerometers used to obtain the measurements were located along the central axis of the car, spaced approximately 12.42 m apart. Measurements were taken at 300 samples per second and post processed with an anti-aliasing algorithm to ensure an accurate reconstruction of the true signal up to 100 Hz from the digitized measured data.

Phase 3 (P3) loads were extracted from a set of data files received from TTCL on August 13, 2013. Each data file contained a variable duration (multi-tens-of-minutes) snapshot of rail car acceleration time-history data produced by the NUCARS[®] [12] software for a single eight-axle, drop-center, rail car (whose design is based on a preliminary for a rail car that would meet the Association of American Railroads (AAR) S-2043 Standard [15]) as it traversed an approximately 25-mile representative segment of track (referred to as Track 9 by TTCL) at various speeds. The rail car in the NUCARS[®] simulation was loaded with a transportation cask consistent with the cask

assembly FEM described later. Acceleration time-histories (consisting of all six degree-of-freedom accelerations at the cradle-to-rail-car interface, sampled at 150 samples per second) were provided for velocities of 10, 20, 24, 30, 40, 50, 53, and 62 mph.

Due to the limitations placed on the length of time that can be effectively simulated using explicit FE analyses (as described earlier in the discussion of the selection of the P1 load cases), ten-second duration load cases were extracted from the longer NUCARS[®] snapshots provided by TTCI. A total of five load cases were produced. Two load cases were designated as shock load cases, and are ten-second duration excerpts from the longer NUCARS[®] snapshots that capture the most severe transient shock event in each of the three directions. Only two distinct shock load cases were produced. This is because the worst case axial and vertical shocks occur nearly simultaneously and within the same ten second excerpt, thus negating the need for a separate load case for each of these shock events. The remaining three load cases were designated vibration load cases, and are ten second duration excerpts from relatively shock free sections of the longer NUCARS[®] snapshots that contained average power spectral densities for accelerations in each of the three directions.

The data supplied by TTCI for the P3 loads provides six degree-of-freedom accelerations at a single node located at the interface between the cradle and rail car deck. As was done for the P1 load cases, modifications were made to each load case acceleration time-history to remove large rigid body displacements. This modification was performed in a manner analogous to that performed for the P1 load cases. All of the load cases were taken from the Track 9 snapshot at 62 mph. This snapshot was assumed to represent the most conservative of those provided.

MODEL VALIDATION

Significant validation was performed on the input and modeling that made up the initial demonstration.

In order to validate the predictions that would later be provided by NUCARS[®] identified at P1 and P3 loads, TTCI conducted NUCARS[®] simulations of a railcar with similar characteristics to the representative railcar for which archived data was available. The result of these simulations was that there is a good comparison between modeling and test results for lateral and vertical accelerations [13].

The SNL fuel assembly shaker table test campaign offered a source of validation data for the PWR fuel assembly model. The test campaign subjected a surrogate fuel assembly to shock acceleration loads while the surrogate fuel assembly was instrumented with a number of accelerometers and strain gauges. Comparison of the body of recorded test data to the calculated model results offered quantifiable evidence of the model's ability to predict realistic response of the key areas of dynamic response of the fuel assembly and local strains. A detailed report of the shaker table modeling is provided by Klymyshyn et al. [14] and shows that the assembly-level model is in reasonable agreement with the shaker table data.

The input material properties and the failure limits were validated against a significant body of test data taken on samples that were as representative of the conditions of used nuclear fuel as possible. Test programs are currently underway to expand this database to provide further confirmation of these properties.

RESULTS OF INITIAL DEMONSTRATION

Results of the initial demonstration are provided in this section, including results from the cask-level modeling, the fuel rod-level modeling, and the assembly-level modeling. Based on the results of these models, the fuel rods were assessed against the selected failure criteria.

For the cask assembly as currently realized in the cask assembly FEM [2], the shock and vibration loads derived from the P1 data provided by TTCI produce significant excitations at the fuel assembly-level. In the axial and vertical shock cases, the rail car loads are sufficient enough to result in slip and/or vertical separation of the fuel assemblies in the basket and impact of the fuel assemblies against either the basket cell walls or the top or bottom spacer blocks. Based on this observation alone, the P1 transportation loads as realized in the selected load cases appear to be severe enough to be of concern. However, detailed modeling at the fuel assembly-level is required to definitively assess this. It is worth noting that the P1 shock load in the vertical direction is consistent with the shock environment defined for truck transport as described in NUREG/CR-0128 and therefore may be some indication of the severity of the truck transport shock loading environment. P1 vibration loads, while somewhat more benign with respect to their ability to produce fuel assembly slip and vertical separation than the P1 shock loads, still tend to produce excitations at the fuel assemblies of significant magnitude in the frequency range of concern, namely between 10 and 40 Hz, that further modeling at the detailed fuel assembly-level is required to assess these loads for their severity.

For the cask assembly as currently realized in the cask assembly FEM, the shock and vibration loads derived from the P3 data provided by TTCI produce excitations at the fuel assembly-level significantly reduced from those of the P1 shock load cases. However, the P3 shock loads are still sufficient enough to induce sliding of the fuel assemblies in the basket and impact of the fuel assemblies against either the basket cell walls or the top or bottom spacer blocks. Based on this observation, and the sensitivity of the response severity to component-to-component gap size, the P3 transportation loads as realized in the selected load cases appear to have the potential to be severe enough in some instances to be of concern. Detailed modeling at the fuel assembly-level is required to definitively assess this. Also, additional sensitivity studies are required to more fully quantify the importance of uninvestigated parameters such as coefficients of friction between interacting bodies, structural damping, analytical handling of contact within the FE code, input load characteristics, and design details of the cradle-cask-canister-basket assembly on the severity of the load environments generated at each fuel assembly. Finally, while the P3 vibration loads are generally more benign than the P1 vibration loads, they still produce excitations at the fuel assemblies of significant magnitude in the frequency range of concern for the fuel assemblies that detailed fuel assembly-level modeling to assess their import is warranted.

The rod-level analysis provides best estimate stiffness and damping properties of a high burn-up fuel rod based on nominal dimensions [4]. It also quantifies the range of flexural rigidity of high burn-up fuel based on various bounding conditions between the pellet-pellet and pellet-clad interface. This range of fuel rod flexural rigidity defines the material property uncertainty range which is used to broaden assembly-level response spectra. Time histories are generated to fit these broadened response spectra and used as input to the assembly-level PWR analysis.

At the assembly-level, a detailed model of the Westinghouse Electric 17×17 OFA PWR assembly

was constructed in LS-DYNA®^a [3]. Preliminary sensitivity analyses of the various model options were tested by modal analysis to evaluate the effects on natural frequencies of the entire fuel assembly and the individual fuel rods. Preliminary transient dynamic analysis with P1 loading was used to evaluate the fuel rod strain history. The fuel rod stiffness, spacer grid spring stiffness, and spacer grid locations had a strong influence on the assembly and fuel rod natural frequencies and resulting fuel cladding strains. Location of the assembly in the basket and the addition of control components had a smaller but moderate influence on the maximum cladding strains observed in the transient response. Temperature and fuel rod location in the assembly had only a small influence on the natural frequencies and resulting transient response. Transient dynamic cases using P3 loading based on NUCARS® simulation were then performed and indicated that the vertical shock had the most potential for high cladding deformation and strain. Additional transient dynamic cases were also ran with inputs derived from the P3 loading to identify a bounding envelope encompassing the response of all 32 basket compartments and peak broadened to account for uncertainty in the fuel rod stiffness. This loading was significant enough to still cause lateral and axial sliding of the assembly within the basket and impact with the side walls, but the assembly did not separate from the basket floor due to vertical loading. Significant amplification of the assembly response was observed for all cases at frequencies above 40 Hz consistent with the estimated rod natural frequencies of 50-60 Hz. The lateral shock case exhibited the highest cladding strain in the transient dynamic model, but the lateral vibration case had the highest potential fatigue damage.

The predicted cladding strains were not large enough to cause plastic deformation or structural failure, but cyclic strains roughly projected for the entire route were significant in some cases. A rain-flow counting procedure was used to compute the magnitude and number of cladding strain cycles for each fuel rod element in the assembly. These strain cycles are binned and counted for the 10s simulation time. These are extrapolated for a 3000 mile trip and the damage contribution for each strain bin is calculated as the number of cycles the fuel rods hit over the projected 3000 mile journey divided by the critical number of cycles to failure. The total damage for a single rod was then computed by summing the contributions from each of the strain bins. Failure is not expected for damage fractions less than 100%. For the P3 loading without peak broadening, loading was fairly benign and cumulative fatigue damage fraction was less than 1% for all of the cases considered. With the broadened P3 loading, lateral excitations were larger and cumulative fatigue damage for the lateral vibration case was projected to be 11% of the critical value based on the representative 10s window response. The cumulative fatigue damage fraction for the lateral shock case was 7% for a conservative accounting of frequent high amplitude shock events over the entire route. Fatigue damage projections for the vertical shock were 5% while the vertical and longitudinal vibration cases were less than 1%.

The results for the P3 and broadened P3 load cases are shown with the experimental data in Fig. 4. This shows that the results obtained in this effort (which account for the unknown material property variability and location in the basket through the broadened and bounded input definitions) put the cladding much closer to the region where fatigue damage is possible. The argument could also be made that the 11% damage from the lateral vibration case would actually be higher since additional damage will occur from high magnitude shock events. Even if the total damage from the lateral shock and vibration cases are summed, the 18% damage level is still less

^a LS-DYNA is a registered trademark of Livermore Software Technology Corporation in the United States and/or other countries.

than the fatigue threshold. It is also noted that these points are at lower stress/strain levels than that used for the majority of the experimental fatigue tests. Additional data on irradiated specimens for this stress/strain level may be useful to ensure the lower threshold for fatigue strength in this range is adequately captured. Therefore, these analyses show that cladding fatigue damage is predicted to be below the threshold, but additional effort to reducing the assumptions in the failure analysis procedure would be valuable to make a better evaluation of cumulative fatigue damage effects.

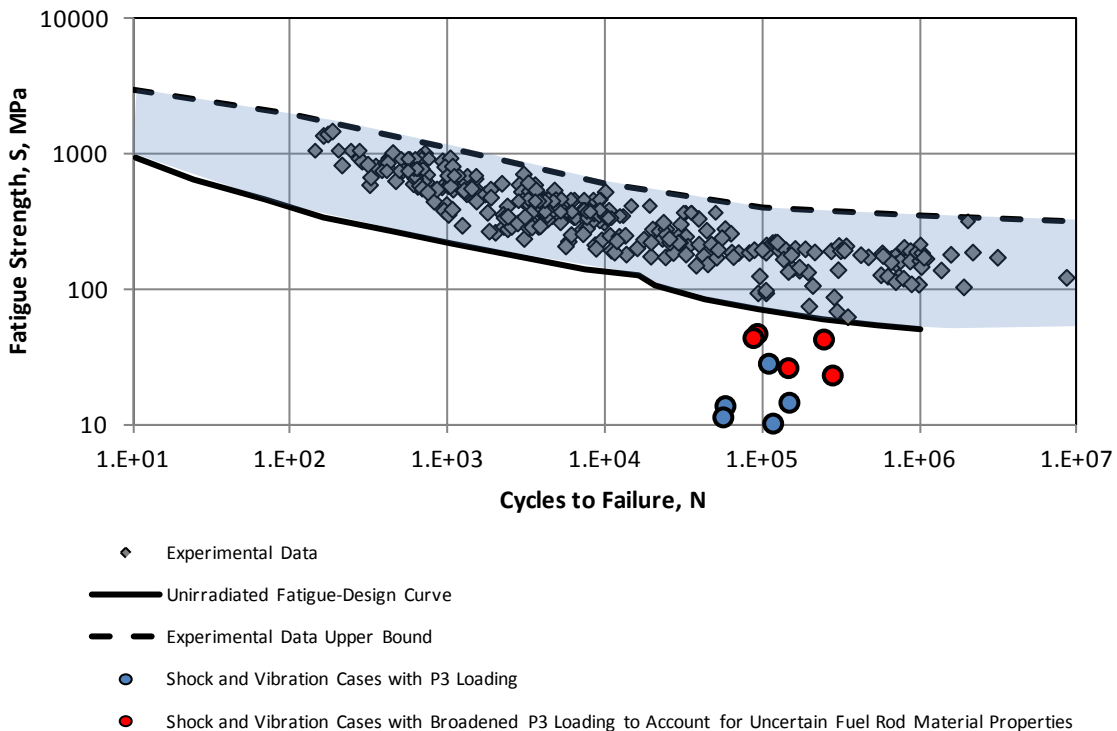


Fig. 4. Clad Fatigue Damage Summary for Shock and Vibration Cases with P3 and Broadened P3 Loading

Therefore, considering that the total damage from summation of the worst shock and vibration cases is ~18% of the expected fatigue limit, the fuel rods do not fail during NCT given the assumptions listed.

SENSITIVITY ANALYSES

Various sensitivity analyses have been identified to evaluate the impact of various material property, initial condition, and modeling uncertainties on the resulting stress and strain predictions, and failure prediction. These analyses guided researchers to focus on areas where uncertainties have a significant impact on the failure predictions.

Sensitivity studies were performed and the results indicate areas of high, moderate, and low sensitivity. The areas of high sensitivity were found to be;

- **Cladding elastic modulus:** Best estimate fuel rod stiffness and damping parameters

were developed at the rod-level analysis and provided to assembly-level analysis. Rod-level analysis also developed a range of fuel rod flexural rigidity (range of material uncertainty). The basket response spectra (generated by the cask-level analysis) are broadened by the range in flexural rigidity uncertainty. Time histories are fit to these broadened response spectra and are used in the best estimate assembly-level analysis. At the assembly-level, modal analysis indicates a wide range of natural frequencies between the upper and lower bound rod stiffness values indicating the importance of the integrity and load carrying capability of the pellet-clad interface. Transient analyses showed cumulative clad damage with broadened P3 loading (18%) was much higher than with unmodified P3 loading (1%), but both are still well below expected failure criteria (100%).

- **Spacer grid stiffness:** Analysis at the rod-level performed to produce equivalent shell thickness that provides similar lateral displacements to one with springs and dimples. At the assembly-level, modal analysis indicated that the spring stiffness values have a strong influence on the natural frequencies of the fuel rods, so different designs and the possibility of spring relaxation or gap formation could significantly influence the rod response.
- **Spacer grid location:** Larger grid-to-grid distance gives a longer unsupported fuel rod span with a lower natural frequency that leads to higher bending strains in the vicinity of the spacer grid.
- **Gaps between the assembly and the cask:** For loads consistent with the P3 shock loads and for the range of clearances investigated, the gaps are of significant importance in determining the severity of the excitations at each fuel assembly, particularly for excitations in the lateral and axial rotation directions.

The areas of moderate sensitivity are;

- **Fuel assembly basket location:** Basket location matters moderately for the assembly loading, so methods to provide a bounding case for all of the basket compartments would be advantageous to ensure the worst basket location has been evaluated.
- **In-reactor fretting wear:** Increase or decrease in nominal bending stress calculated and a multiplier is provided to the assembly-level model to account for this. The multiplier is approximately 1.41 times the bending stress.
- **Influence of control components:** The added mass and stiffness at the top of the assembly from inclusion of the control assembly resulted in lower strains for the cladding.
- **Pellet-to-clad bonding:** Increase or decrease in nominal bending stress is calculated and a multiplier is provided to the assembly-level model to account for this. The multiplier is approximately 1.38 times the nominal bending stress.

The areas of low or no sensitivity are;

- **Cladding yield stress:** The anticipated range of yield stress for either irradiated or unirradiated cladding are well above expected cladding bending stress.
- **Fuel rod location in assembly:** Little evidence has been observed in the various cases so far to suggest that different fuel rods locations in the spacer grids behave significantly differently from each other under NCT conditions.
- **Temperature distribution:** The effects of temperature on the materials' elastic moduli (not including the fuel rod itself) had a small effect on the response and cladding strains.

WM2014 Conference, March 2 – 6, 2014, Phoenix, Arizona, USA

- **Fuel rod damping:** Damping was determined to be minimal in the fuel rods. However, the Rayleigh damping parameters provided to the assembly-level analysis was determined by varying the coefficient of friction and bonding at the pellet-pellet and pellet-clad interfaces.
- **Pin pressure influence:** Internal pin pressure influence reduces the stress concentration caused by pellet-to-clad bonding and in-reactor fretting wear. Therefore this effect was not considered in the final analysis

CONCLUSIONS

A detailed modeling approach and basis for simulating UNF under NCT has been developed and used in an initial demonstration. This approach includes five main modeling inputs;

- Simulated loading histories of an AAR specification S-2043 rail conveyance [15]
- Component material properties including irradiated fuel and cladding properties
- Component temperatures
- Fuel and assembly post-irradiation conditions
- Cask, canister, and fuel assembly geometry

The modeling approach includes three main levels [2, 3, and 4];

- Cask-level modeling
- Fuel assembly-level modeling
- Fuel rod-level modeling.

The strains in the fuel rods produced by these models were compared to fatigue failure criteria to assess the possibility for damage during the expected rail journey.

Extensive validation was performed on the model inputs, the FEA models, and the fatigue failure criteria to demonstrate the validity of the results.

Results of an initial demonstration involving moving high burnup Westinghouse Electric 17x17 OFA fuel in a GBC-32 on a 3000-mile rail journey have been provided. It was determined that peak cladding strains were not large enough to cause plastic deformation or structural failure, but cyclic strains roughly projected for the entire route were significant in some cases. The damage ratio for a 3000-mile route was calculated based on a conservative accounting of the vibration and shock loading derived from the representative 10s simulation cases. The total damage for a single rod was then computed by summing the contributions from each of the strain bins. Failure is not expected for damage fractions less than 100%. Cumulative fatigue damage fraction was projected to be 11% of the critical value for the lateral vibration case and 7% for the lateral shock case. Conservatively assuming that the high amplitude shock events occur concurrently with the continuous vibration, the total projected damage is 18% of the critical value. Therefore the fuel rods do not fail during NCT for this demonstration.

Sensitivity studies were performed and the results indicate areas of high, moderate, and low sensitivity. The areas of high sensitivity were found to be, cladding elastic modulus, spacer grid stiffness, spacer grid location, and gaps between the assembly and the cask. The areas of moderate sensitivity are, fuel assembly basket location, in-reactor fretting wear, influence of

control components, and pellet-to-clad bonding. The areas of low or no sensitivity are, cladding yield stress, fuel rod location in assembly, temperature distribution, fuel rod damping, and pin pressure influence.

REFERENCES

1. H. ADKINS, K. GEELHOOD, B. KOEPEL, J. COLEMAN, J. BIGNELL, G. FLORES, J.A. WANG, S. SANBORN, R. SPEARS, and N. KLYMYSHYN, "Used Nuclear Fuel Loading and Structural Performance Under Normal Conditions of Transport – Demonstration of Approach and Results on Used Fuel Performance Characterization", September 30, 2013 FCRD-UFD-2013-000325.
2. J. BIGNELL, G. FLORES, and D. AMMERMAN, "Cask Assembly Level Modeling to Determine Used Nuclear Fuel Assembly Loading Environments Resulting From Normal Conditions of Rail Transport (14511)," *WM2014 Conference*, Phoenix, Arizona, USA, March 2-6, 2014.
3. S. SANBORN, B. KOEPEL, N. KLYMYSHYN, H. ADKINS, and K. GEELHOOD, " Assembly Level Modeling and Transportation Damage Prediction of Used Nuclear Fuel (UNF) Cladding (14569)," *WM2014 Conference*, Phoenix, Arizona, USA, March 2-6, 2014.
4. J. COLEMAN, and R. SPEARS, "Detailed PWR Fuel Rod and Grid Finite Element Analysis to Provide Equivalent Rod Stiffness and Damping and Equivalent Grid Shell Thickness to PWR Used Nuclear Fuel (UNF) Assembly (14525)," *WM2014 Conference*, Phoenix, Arizona, USA, March 2-6, 2014.
5. J.A. WANG and H. WANG, B. Revard, and R. Howard, "Reversal Bending Fatigue Testing on Zry-4 Surrogate Rod (14503)," *WM2014 Conference*, Phoenix, Arizona, USA, March 2-6, 2014.
6. J WAGNER, "Computational Benchmark for Estimation of Reactivity Margin from Fission Products and Minor Actinides in PWR Burnup Credit", 2001, NUREG/CR-6747, ORNL/TM-2000/306.
7. K. GEELHOOD, "Used Nuclear Fuel Loading and Structural Performance Under Normal Conditions of Transport – Supporting Material Properties and Modeling Inputs." 2013, FCRD-UFD-2013-000123.
8. K. GEELHOOD, W. LUSCHER, and C. BEYER, "FRAPCON-3.4: A Computer Code for the Calculation of Steady-State, Thermal-Mechanical Behavior of Oxide Fuel Rods for High Burnup", 2010, NUREG/CR-7022, Vol. 1, PNNL-19418, Vol. 1.
9. K. GEELHOOD, W. LUSCHER, C. BEYER, and J. CUTA, "FRAPTRAN 1.4: A Computer Code for the Transient Analysis of Oxide Fuel", 2010, NUREG/CR-7023, Vol. 1, PNNL-19400, Vol. 1.
10. H. ADKINS, J. CUTA, B. KOEPEL, A GUZMAN, and C. BAJWA, "Spent Fuel Transportation Package Response to the Baltimore Tunnel Fire Scenario", 2006, NUREG/CR-6886 Rev. 1, PNNL-15313.
11. H. ADKINS, "Used Nuclear Fuel Loading and Structural Performance Under Normal Conditions of Transport – Modeling, Simulation and Experimental Integration RD&D Plan", 2013, FCRD-TIO-2013-000135.
12. TTCL - Transportation Technology Center, Inc., "NUCARS® Help Manual, Version 2013.1", 2013.
13. C. URBAN, N. WILSON, and A. Keylin, "NUCARS® Modeling Support for DOE Used Nuclear Fuel Disposition, Task 2: NUCARS® Simulation of Representative Railcar", 2013, ORNL-13-002.

WM2014 Conference, March 2 – 6, 2014, Phoenix, Arizona, USA

14. N. KLYMYSHYN, S. SANBORN, H. ADKINS, AND B. HANSON, “Fuel Assembly Shaker Test Simulation”, 2013 PNNL-22507.
15. AAR - Association of American Railroads, “Standard S-2043 Performance Specification for Trains Used to Carry High-Level Radioactive Material”, 2003, (DIRS 166338).

ACKNOWLEDGEMENTS

The authors would like to thank John Wagner and Rob Howard (Oak Ridge National Laboratory) for instilling the concept of evaluating moderate to high burnup fuel under conditions of normal transport. The authors would also like to thank John Orchard, Ned Larson, and the U.S. Department of Energy for providing funding for this initiative.